ELSEVIER

Journal of Nuclear Materials 273 (1999) 117–129

journal of nuclear materials

www.elsevier.nl/locate/jnucmat

# TEM and SEM studies of radiation blistering in helium-implanted copper

P.B. Johnson *, R.W. Thomson, Karen Reader

*School of Chemical and Physical Sciences and Electron Microscope Facility, Victoria University of Wellington, P.O. Box 600, Wellington, New Zealand*

Received 13 July 1998; accepted 19 February 1999

**Abstract**

Nanoporous layers produced in metal surfaces by He implantation are of special interest for applications such as catalysis. At high doses nanoporous layer formation can be limited by the onset of radiation blistering. Research into the blistering of metals was stimulated originally by the need to find materials resistant to blistering for use in the first-wall of future nuclear fusion reactors. Blistering was the subject of intensive international study in the two decades centred on 1977. Despite this effort the bubble structures associated with blistering were never determined. In the present work TEM sections have been successfully prepared, by ultramicrotomy, perpendicular to the surface of high dose copper targets. For the first time, in any case of radiation blistering, the bubble structures directly associated with blistering are identified and their depth dependence determined. Local swellings, caused by a bimodal distribution of nanoscale bubbles, are estimated to exceed 150%. Probable answers can now be provided for some longstanding questions from earlier studies. 

## 1. Introduction

Nanoporous bubble structures with striking features can be produced in some metals by means of high-dose helium implantation at temperatures $\simeq 0.2T_m$ (where $T_m$ is the melting temperature of the metal). These structures [1], which may be a universal response for all metals implanted under appropriate conditions, show considerable promise in relation to potential applications such as catalysis [2–4]. They are characterised by nanoscale cavities of uniform size, a high degree of swelling and extremely thin metal walls ($\simeq$1 nm in thickness) separating nearest neighbour cavities. The internal surface area associated with the cavities is high and the method of production offers the potential for controlling the pore size through the selection of implantation parameters such as helium energy, dose level and target temperature. To obtain sufficiently thick layers for transmission electron microscopy (TEM) and for oxidation studies, helium energies have usually been chosen in the range 60–160 keV. For monoenergetic implantations the highest helium doses that can usefully be used are limited by disruption of the surface layer by the onset of radiation blistering of the metal surface [2,4].

The radiation blistering of metals subjected to helium irradiation has been intensively studied. These original studies were based mainly on examining surface topography using scanning electron microscopy (SEM). Despite the many studies some important questions still remain concerning the bubble structures at the high helium doses where radiation blistering occurs. These questions include: (i) What is the detailed structure of the bubble (or defect arrays) associated with the high values of swelling found in surface displacement measurements? (ii) What bubble structures are the immediate precursors of radiation blisters appearing on the implanted surface? (iii) Why does the implanted layer become permeable at a critical helium dose level (as suggested by the helium depth profiling and other studies of Terreault et al. [5–7])?

The present work was undertaken to determine the bubble structures at high helium dose levels and so

* Corresponding author. Tel: +64-4 472 1000; fax: +64-4 495 5237; e-mail: Peter.Johnson@vuw.ac.nz

0022-3115/99/$ – see front matter 
PII: S0022-3115(99)00046-X

identify the bubble structures directly associated with radiation blistering. A particular aim was to determine the highest swellings that can be produced in nanoporous layers by monoenergetic helium implantation. A second aim was to re-examine some of the results of early research on radiation blistering, in the light of the most recent work on helium bubble structures.

## 2. Previous research

### 2.1. Evolution of bubble structure with dose

At low and medium helium doses in metals implanted at low temperatures ($T \simeq 0.2T_m$) the bubbles order to form a gas-bubble superlattice. Superlattice formation [1,8] has been the subject of many studies based on TEM. These studies have been stimulated by the expectation that clarifying the basic mechanisms leading to bubble ordering could make a unique contribution to the understanding of radiation damage processes more generally. Over a range of metals, and different crystal types, it has been found that the bubble superlattice has the same symmetry as the host metal and has principal axes aligned along low index directions in the metal [1,8]. The bubble concentrations in superlattices can be very high. For example, in vanadium implanted at room temperature [9], bubble concentrations of $3.6 \times 10^{25}$ m$^{-3}$ have been observed.

A review of work up to 1990 has been given by Johnson [1]. In a subsequent paper, a new study for the body centred cubic (bcc) metals has been reported and research up to 1995 reviewed [9]. A theoretical analysis of the TEM imaging of small superlattice bubbles (diameter $\simeq$2 nm) in copper has been completed [10]. The existence of a lower temperature threshold for bubble ordering in molybdenum has recently been demonstrated [11].

Previous research supports the following model for the evolution of the bubble structure with increasing helium dose [1,12]. Bubbles nucleate initially to form a random array. As the concentration of helium in the surrounding matrix increases, bubble sizes increase monotonically and patches of order develop in localized regions. The gas-bubble superlattice stage is associated with local helium concentrations $\simeq$10 at.%; typical bubble sizes are $\simeq$2 nm and bubble lattice parameters are $\simeq$6 nm. At helium concentrations just beyond the superlattice stage the bubble array retains some degree of order as it coarsens through the coalescence of nearest-neighbour bubbles. In this partially ordered stage bubble diameters are typically 3–4 nm [1,4]. For local helium concentrations approaching 20 at.% the bubble array has a cellular structure with most bubble cavities still separated from their neighbours. Increases in the local helium concentration beyond $\simeq$20 at.%, cause the bubble array to coarsen further until the size of the most commonly occurring bubbles reaches 6–8 nm. In this stage there is an increasing degree of interconnection between bubble cavities. The bubble structures in this stage are referred to as either cellular or nanoporous depending on the estimated degree of interconnection [1–4,12].

The bubble structures for helium concentrations much beyond $\simeq$20 at.%, through to the critical concentrations $\simeq$30 at.% needed for radiation blistering, have not been previously determined. One major limitation has been the difficulties in preparing satisfactory TEM specimens from highly swollen radiation-hardened layers on soft substrate metal.

### 2.2. Radiation blistering

Much of the previous research into the radiation blistering of metals under helium ion-irradiation was motivated by the need to find materials resistant to blistering for use as the primary containment wall of future controlled thermonuclear fusion reactors (CTRs). For most metals, and most implantation temperatures, helium is insoluble and precipitates out to form gas bubbles in high concentration. Bubble structures and radiation blistering have been the subject of regular reviews, for example [1,13–17]. SEM examination has shown that the blisters that form on metals such as copper, when irradiated to high helium dose levels at temperatures $T < 0.35T_m$, are commonly regular, discrete and dome-shaped with diameters about 5–10 μm. In 'classical' blistering of this kind the thickness of the blister lid shows little variation from one blister to the next.

Yadava [18] has summarised the effect of temperature on the development of surface topography under monoenergetic (inert) ion bombardment. Three broad temperature ranges are distinguished: (i) $T < 0.25T_m$ – typically well-shaped (classical) blisters form suddenly at the 'critical dose' (see, for example, [13,20]), (ii) $0.25T_m < T < 0.44T_m$ – the level of blistering and exfoliation/flaking is largest, and (iii) $T > 0.50T_m$ – the degree of blistering decreases with increasing temperature and at high temperatures a sponge-like surface structure develops. The present work investigates the bubble structures associated with classical blistering in copper induced by helium irradiation at a temperature $\simeq 0.2T_m$.

### 2.3. Transverse TEM sections

Transverse sections have the advantage that the depth of structures below the surface can be directly measured from TEM micrographs. Relationships between bubble structures at different depths can be investigated in the same specimen and compared under identical imaging conditions in the same micrograph. The spatial arrangement and shape of bubble images can be examined in projections on planes normal to the implanted surface. Previously, transverse sections have

been successfully prepared from copper implanted to low and intermediate helium dose levels [12] but not from metals implanted to high dose.

Copper was chosen for this study for several reasons: (i) the physical and chemical properties of copper are well researched and documented and in this sense copper can be regarded as a model metal (ii) the response of copper to helium implantation has been found to be representative of many metals [1,2,4,9], (iii), copper has been used in many previous studies [1,19] including research on radiation blistering [20–22] and on the dependence on depth of the bubble structures at low and intermediate helium dose levels [12,23], and (iv) copper was used in the most comprehensive helium depth-profiling studies related to radiation blistering [5–7].

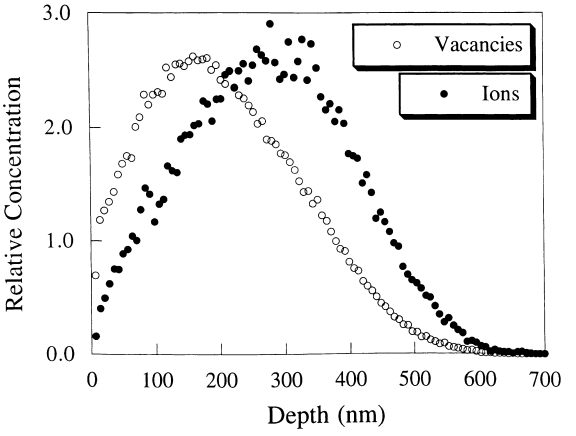


Fig. 1. Helium and damage depth profiles in Cu, calculated using the Monte Carlo computer programme TRIM-95. Depths are normal to the specimen surface. Vertical scales are in arbitrary units. Solid circles give the ion end-of-range distribution. Open circles give the damage in terms of the number of interstitial-vacancy pairs.

## 3. Experimental

### 3.1. Implantation conditions

The targets were prepared from very thin (≃25 μm) copper foil to reduce cutting difficulties in preparing thin TEM sections by ultramicrotomy. The high purity, polycrystalline foils were heat-treated in vacuum, mechanically polished and then electropolished to a high surface finish immediately prior to implantation. To spread the implanted helium over a large depth range, a relatively high helium energy (160 keV) was chosen. An oblique angle of incidence of the ion beam (60° to the surface normal) was used to improve the uniformity of the distribution of helium with depth. Under these conditions the helium profile is a broad bell-shaped curve centred on a depth equal to the mean projected range, $R_p \simeq 270$ nm, as shown in the calculated profile of Fig. 1. The calculated damage profile, shown for comparison in the Fig. 1, is also a broad bell-shaped curve but is centred on a depth ≃150 nm. The data for Fig. 1 were obtained using the Monte Carlo computer programme TRIM-95 (Ziegler, IBM-Research [24]). The helium implantations were at a temperature of 320 K and to dose levels sufficient to cause radiation blisters to form on the target surface. The critical dose for blistering, $\phi_c \simeq 1.5 \times 10^{22}$ $He^+$ $m^{-2}$, corresponds to helium loadings at depths around $R_p$ in the region of 30 at.%. Also, some lower dose implantations were done ($1.2 \times 10^{22}$ $He^+$ $m^{-2}$) to link the high dose results obtained here to the lower dose regime covered in earlier work [12]. Radiation blisters on the 'as-implanted' surfaces were examined by scanning electron microscopy in a Philips 505 SEM.

### 3.2. TEM sectioning by ultramicrotomy

Ultramicrotomy was used to prepare electron transparent sections perpendicular to the implanted surface (i.e. transverse sections) from high dose targets. The implantation details and cutting techniques used are similar to those reported previously [12] for low and intermediate dose targets and so only a brief description is given here. Narrow wedges were cut from the implanted foil with a scalpel blade held perpendicular to the implanted surface. These were approximately 5 mm in length and 2 mm wide at the base, tapering to a fine point to ensure the area of metal to be sectioned was as small as possible. The cutting procedure is described below with reference to Fig. 2.

Each wedge of metal was embedded in resin (Procure 812). After curing, the face of the resulting block was trimmed to a trapezium shape with the implanted surface of the metal perpendicular to the parallel sides. When the block is mounted in the ultramicrotome, this arrangement gives a cutting direction that is parallel to the implanted surface (i.e. perpendicular to the surface normal). This direction, the $X$ direction of Fig. 2, was chosen to minimize the cutting forces in the $Z$ direction (i.e. along the surface normal).

The sectioning was done on a Reichert–Jung Ultracut E ultramicrotome. Several sections were cut with a glass knife to produce a smooth block face prior to cutting the ultra-thin sections with a diamond knife at a clearance angle of 4°. A cutting speed 1.5 mm $s^{-1}$ was chosen to minimize the specimen curling encountered at lower speeds. The ultra-thin sectioning feed was set to 30 nm or to the lowest setting that would produce satisfactory sections. The sections, cut perpendicular to the implanted surface, were picked up on 400 mesh copper grids that were either uncoated or coated with a holey carbon film.

To measure the thickness of the microtomed sections, a few grids containing sections were re-embedded and

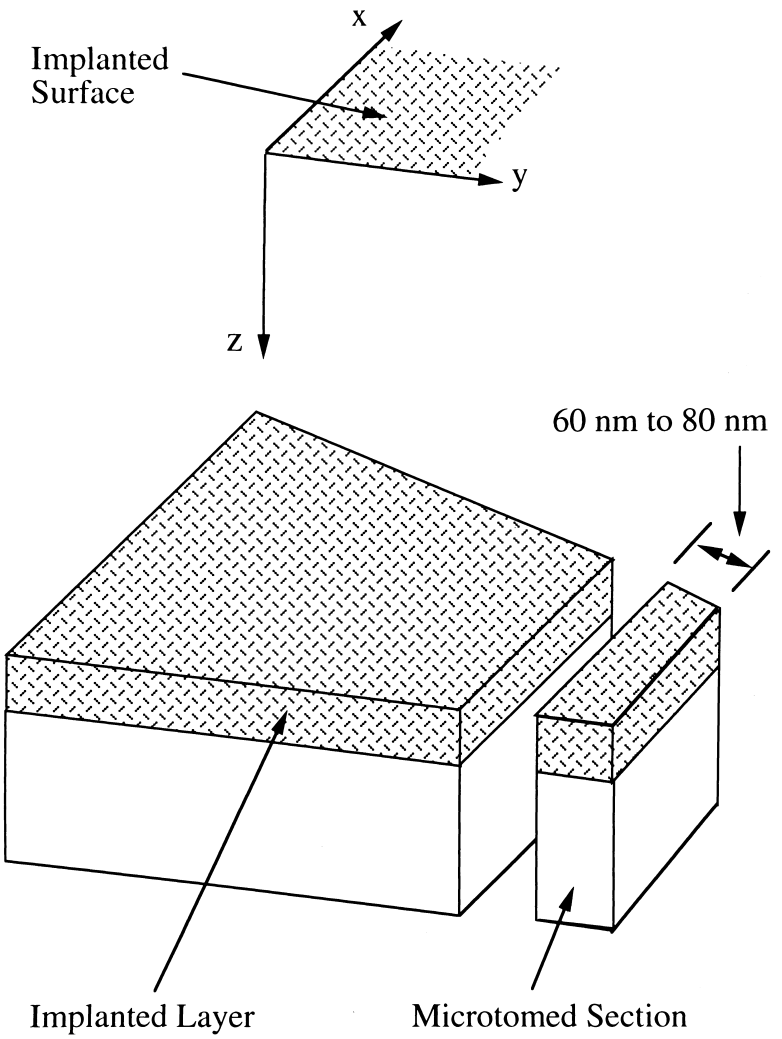


Fig. 2. Thin sections are produced perpendicular to the implanted surface (transverse sections) by means of ultramicrotomy. A coordinate system is adopted where the *Z*-axis is perpendicular to the implanted surface and the *Y*-axis is normal to the plane of the thin section. The cutting direction is along the *X*-axis. TEM examination is with the electron beam directed down the *Y*-axis.

sectioned in a direction perpendicular to the long axis of the original section. The thicknesses were then determined by TEM examination. Typical thicknesses were 60–70 nm. Images of the bubbles in the transverse sections were recorded at high magnification in both under- and over-focus conditions in bright field in a Philips EM 420ST 120 keV TEM.

## 4. Results and discussion

### *4.1. Blister morphology*

The radiation blisters on copper surfaces are shown in Fig. 3. The results are broadly similar to those of the early studies summarised in Ref. [13]. Discrete blisters are formed with sizes in the range about 5–8 μm across; there is no preferential decoration of grain boundaries (Fig. 3(a)). In some cases, blister lids have been blown off to reveal highly pitted cavity floors (Fig. 3(b)). In Fig. 3(c) two similar blisters are shown, one with the lid partially raised to reveal the edge of the lid and the other with the lid missing to expose the crater below. Measurements made on the edges of the lid and crater suggest that the lid thickness is $\simeq$500 nm. This estimate is subject to a large uncertainty because of the high swellings involved and the imprecise definition of lid and crater edges. There is also the possibility that lid thicknesses measured at the lid edge are not representative of the lid thicknesses away from the edge.

The structures within crater floors and crater edges are shown in detail in Fig. 3(d)–(f). In the plane of the

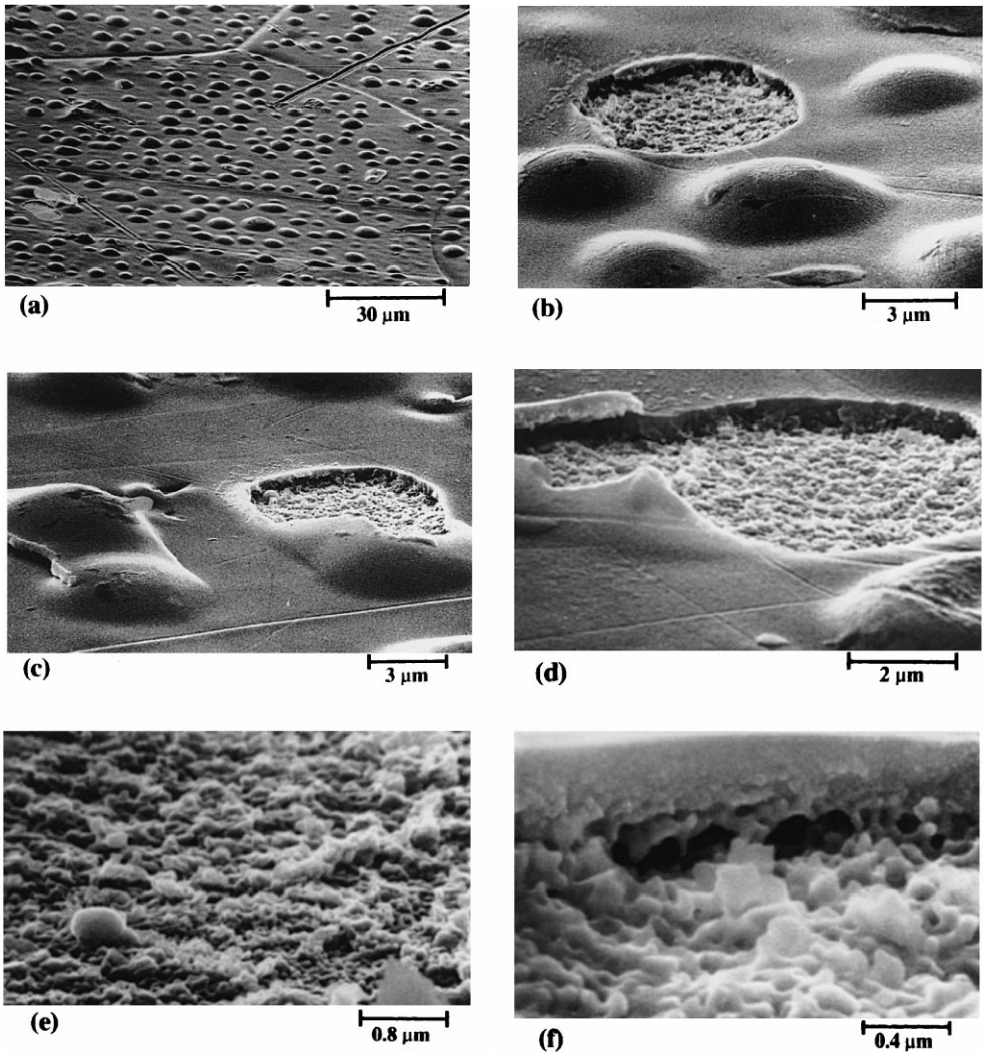


Fig. 3. SEM micrographs of radiation blisters in copper produced by high dose helium implantation to the critical dose for radiation blistering. (a) A general view of the surface at low magnification. Several grain boundaries are evident, e.g. the three grain boundaries meeting at a point near the top of the picture. (The two large scratches on the surface are from diamond polishing.) Blister morphology appears to be independent of grain orientation. (b) Five intact blisters near a blister crater. (c)–(f) Detailed views of the bubble structures in the floors of blister craters.

crater floors there are discrete cavities in high concentration with diameters in the range 40–80 nm. The metal pillars and other debris standing up from the crater floor are typically from 100 to 300 nm across. The diameters of the cavities revealed in crater edges, above the level of the crater floors, lie in a similar size range. The aim of the TEM study of transverse sections is to clarify the nature of these structures for helium dose levels $\phi \simeq \phi_c$.

### 4.2. Bubble structures for $\phi < \phi_c$

A TEM micrograph of a bubble array viewed in transverse section is shown in Fig. 4. The distribution of bubble sizes with depth follows approximately a bell-shaped curve similar to the variation in helium concentration with depth given in Fig. 1. The bubble sizes reach a maximum at a depth of approximately 300 nm. At these depths, around the centre of the calculated maximum in the helium concentration profile, the bubble structure has a cellular appearance with cavity sizes in the range 3–5 nm. Planar sections prepared parallel with the specimen surface have shown that these bubbles are sufficiently well ordered to give rise to diffraction satellites [4]. Although bubble ordering is not an obvious feature of the bubble arrays in micrographs such as Fig. 4, this is readily explained by the plane of the


Fig. 4. A TEM micrograph of a transverse section from Cu following implantation to an intermediate dose level $\simeq 1.2 \times 10^{22}$ $He^+$ $m^{-2}$ at a temperature of 320 K. This dose level is insufficient to cause radiation blistering. The bubble sizes increase with increasing depth to reach a maximum at a depth of $\simeq$300 nm. Typical bubble sizes at this depth are 3–5 nm diameter.

transverse section (the $XZ$ plane) not corresponding to a major crystal plane in the copper [12].

Bubble shapes viewed in projection on $XZ$ planes in transverse sections seem identical to those viewed on $XY$ planes in parallel sections [12]. Bubble facetting is evident in both types of projection. For cavities with sizes less than 6 nm, apart from the effects of facetting, bubble cavities are on average approximately spherical. For the individual bubbles that depart from a spherical shape, the axes of elongation show no preferred direction relative to the surface normal. These results agree well with those of our previous study [12] for this intermediate dose range.

### 4.3. Bubble structures for $\phi = \phi_c$

#### 4.3.1. Bubble precursors to blistering

For this high dose level, $\phi = \phi_c$ ($\simeq 1.5 \times 10^{22}$ $He^+$ $m^{-2}$), about 10% of the sections cut yielded satisfactory transverse TEM specimens. A typical TEM micrograph is shown in Fig. 5. The area selected corresponds to a region between blisters. A striking feature is the large bubbles ranging in size from 30 to 80 nm, or more, across. These large bubbles cover a broad depth region extending from a depth $\simeq$200 nm through to $\simeq$510 nm. When allowance is made for the effects of swelling, this band of large bubbles is centred on a depth of $\simeq$270 nm in compact (unswollen) copper, i.e. the depth of maximum helium concentration.

Most of the large bubbles appear to be facetted to some degree. Where individual bubbles are elongated, the axes of elongation show no preferred direction relative to the surface normal. Analysis of the facetting directions suggests that the section in Fig. 5 may be from a (1 1 0) grain and that the normal to the plane of the section is probably, within broad uncertainties, along [1 $\bar{1}$ 0]. The main facetting planes evident in Fig. 5 are then (0 0 2), (1 1 0), (1 1 1) and (1 1 $\bar{1}$). The concentration, size and facetting of the large bubbles are similar to those found for bubbles formed by the post implantation thermal annealing of a pre-existing gas-bubble superlattice at a temperature $\simeq$700 K ($\simeq 0.5T_m$) [25,26]. This similarity of bubble structure raises the question as to the effective temperature in the highly cavitated buried layer over the later stages of implan-

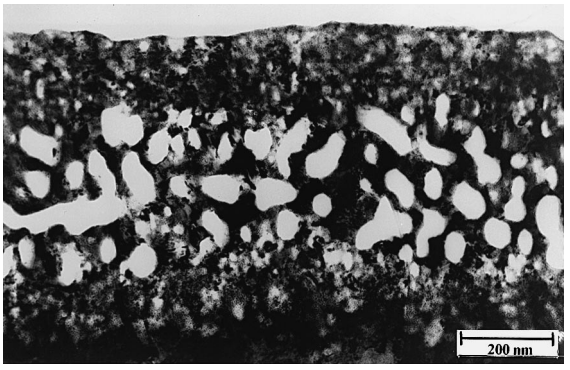


Fig. 5. A TEM micrograph of a transverse section from Cu following implantation to a high dose level $\simeq 1.5 \times 10^{22}$ $He^+$ $m^{-2}$ at a temperature of 320 K. At this dose level radiation blisters have formed on the surface. (Note that the magnification is different from that in Fig. 4.) In a broad depth region centred on 300 nm the bubbles are now much larger, ranging in size from 30 to 80 nm across.

tation. This question is discussed further in Section 5.5.3.

Several other features are worthy of note. There are no local distortions of the surface to match the underlying large bubbles. When viewed from above in the SEM the surface in regions between blisters appears undisturbed and gives no hint of the large bubbles in high concentration beneath. These results indicate that in effect the swelling has been accommodated by a global upward displacement of the surface, rather than by local distortions of the surface on the scale of the individual large bubbles.

The metal columns between the large bubbles contain smaller bubbles in high concentration. Representative micrographs of these smaller bubbles are shown in Fig. 6. Although strain and curvature effects limit the quality of the imaging, it is clear that the columns of metal contain the cellular/nanoporous bubble structure that filled the entire central depth region at slightly lower dose levels. The conclusion is that these columns too, as well as the implanted layer as a whole, are highly swollen.

*4.3.2. Blister profile*

Many of the sections have sliced through blister cavities. In none of these cases has the blister lid been retained intact. However, in several cases the 'ramparts' at the edge of the lid, where the lid separates from the basement metal, can be readily identified. Examples are included in the montage of a section through a blister shown Fig. 7. In this case, although the central part of the lid was missing, small sections of lid, the 'ramparts' on either side of the blister, were retained in the transverse section. Large bubbles having the same sizes, shape and spacing, as those in Fig. 5 are evident in the undersides of these ramparts. Whereas there are also some large bubbles in the cavity floor, they are in much lower numbers and tend to be smaller than those in the retained lid fragments. The thickness of the ramparts is $\simeq$450 nm. This agrees well with the value $\simeq$500 nm obtained from measurements made on exposed blister and crater edges in the SEM micrographs of Section 4.1. In Fig. 7, the lateral extent of the blister montage has been foreshortened (by a factor of about four) so as to allow the ramparts to be shown at sufficiently high magnification to reveal details of the bubble structure. To aid comparison with the immediate precursory bubble structure, and to aid visualisation, the blister lid has been 'completed' with a section of micrograph taken from Fig. 5. (The relative magnification has been adjusted accordingly.)

A comparison of Figs. 5–7 leads to the conclusion that a blister forms when the columns between the large bubbles in Fig. 5, fail by cracking to allow the blister cap to be domed up by some combination of gas pressure and lateral stress. The plane of this cracking appears to be at a depth in the range about 450–500 nm. This depth of separation corresponds to the lower edge of the highly swollen region containing the high concentration of large bubbles.

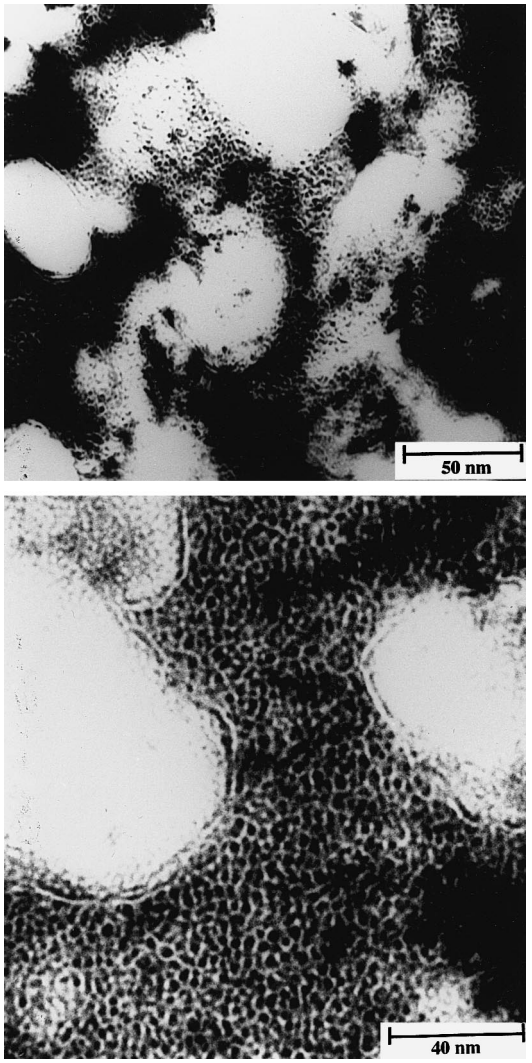


Fig. 6. TEM micrographs of the transverse section of Fig. 5 taken at higher magnification to show the bubble structure in the metal columns between the large bubbles. This structure is shown in relation to the large bubbles in (a) and at higher magnification in (b). Note that the columns contain cellular bubble structures similar to those observed for intermediate dose implantations (see Fig. 4).

*4.3.3. Swelling estimates*

Measurements made on the micrograph of Fig. 5 allow estimates to be made of the swelling in the implanted layer. In Fig. 5 the bubble structure at a depth of 650 nm consists of small bubbles of the size and spacing typical of the gas-bubble superlattice. This type

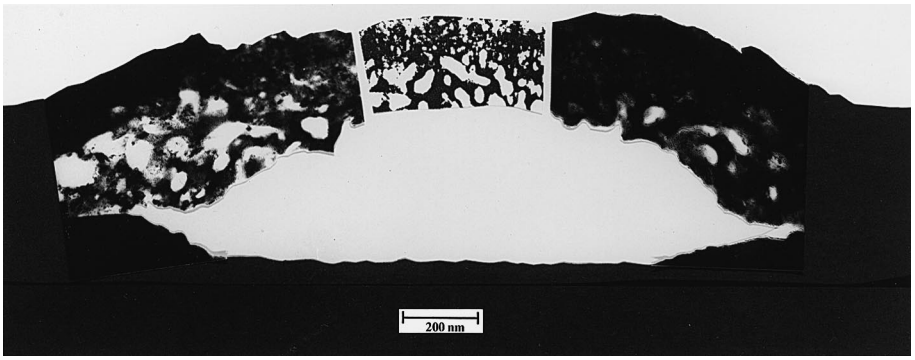


Fig. 7. A montage of three TEM micrographs showing a simulated transverse section through the lid of a typical blister. In a particular transverse section, although the central part of the lid was missing, small sections of lid, the 'ramparts' on either side of the blister, were retained. The horizontal extent of the blister has been shortened to allow the 'ramparts' to be shown at sufficiently high magnification to reveal details of the bubble structure.

of bubble structure is associated with local helium concentrations ≃10 at.% (see Section 2.1). If the data of Fig. 1 are scaled to match the total implanted helium dose of $1.5 \times 10^{22}$ $He^+$ $m^{-2}$, it is found that a loading of 10 at.% corresponds to a depth in compact copper of 460 nm ($\simeq 1.7R_p$). On this basis the degree of swelling, averaged over a depth region extending from the surface to a depth equivalent to 460 nm in compact copper, is ≃40%.

Analysis of bubble sizes and spacings in Fig. 5 shows that almost all the swelling is associated with the depth region from 200 to 510 nm (corresponding to the broad band of large bubbles). Estimates of the swelling associated with the small bubbles lying outside this depth region give values of only 5% to 10%. The swelling in the depth region from 200 to 510 nm (in Fig. 5) can be estimated as follows. Firstly, it is assumed that the metal in the depth range from the surface to 200 nm in Fig. 5 is swollen by ≃8%. A depth of 200 nm in swollen copper corresponds then to a depth of 185 nm in compact copper. Secondly, in relation to the region lying beyond the deeper edge of the broad band of large bubbles, two assumptions are made. For the depth range from 510 to 650 nm in Fig. 5, it is assumed that the copper is swollen by ≃8%. In addition, the depth of 650 nm in the swollen copper is taken to be equivalent to 460 nm in compact copper as suggested by the bubble structures found at this depth in Fig. 5. Thus the depth of 510 nm in Fig. 5 equates to a depth of 326 nm in compact copper. The depth band in compact copper that eventually becomes highly swollen with large bubbles extends from a depth of 185 nm to a depth of 326 nm. This band, which has a height of ≃140 nm (measured along the surface normal), increases in height to 310 nm over the course of implantation. This corresponds to a swelling of ≃120%.

The swelling at depths corresponding to the band of large bubbles can also be estimated by measuring the fractional projected area covered by cavities. This method has been used to estimate the swelling in the heavily cavitated region of lateral extent ≃500 nm at the right hand end of the micrograph of Fig. 5. The local volume swelling associated with the large cavities (typical sizes about 40–160 nm) alone is estimated to be ≃140%. There is also a contribution from the smaller cavities (typical diameters about 4–8 nm) in the metal columns separating the large bubbles. On the basis of projected cavity areas this contribution is estimated to be ≃50%. These two components add together to give a total swelling close to 200% averaged over a region of lateral extent ≃500 nm.

In comparing the two methods used here for estimating the swelling at depths near $R_p$ (depth distribution analysis and projected cavity areas) a difference should be noted. Whereas the first method was used to obtain an average over a region of large lateral extent, the second was biased (deliberately) towards high swelling by choosing a heavily cavitated region of limited lateral extent (≃500 nm) to analyse. Given this difference, the two results are in reasonable agreement and indicate high values of the average swelling (exceeding 100%) at depths near the maximum in the implanted helium concentration. Furthermore, the total swelling at depths near the maximum in the helium profile could rise to as high as 200%, or more, before cracking of the metal columns takes place and blistering occurs.

## 5. Discussion

### 5.1. Specimen preparation

Helium implantation to high dose leads to a thin hardened layer containing a high concentration of cavities formed in the surface of relatively soft basement metal. The buried layer containing large bubbles is highly swollen (up to 200%) with the columns between

the large bubbles having the appearance of a metal foam. It is perhaps surprising that it has proved possible to prepare transverse TEM specimens by ultramicrotomy from such material. It is important to use a cutting direction normal to the $Z$ direction (i.e. normal to the specimen surface). This could be expected because any component of the cutting force in the $Z$ direction will tend to disrupt the implanted layer either by tearing or crushing depending on the sense in which the component acts. For polycrystalline foils a limitation of ultramicrotomy is that in any given grain the plane of the thin section, the $XZ$ plane, is in an arbitrary orientation relative to the crystal lattice. Consequently, it is difficult to investigate bubble ordering in transverse sections prepared in this way [12].

The highly swollen structures, involving very large bubbles separated by nanoporous columns of metal, observed here at high helium doses, would be expected to have a very high chemical reactivity. They would be unlikely to survive in TEM specimens prepared by conventional electrochemical thinning processes, owing to the rapid preferential erosion of the highly cavitated metal. This could explain why these structures were not detected in earlier TEM studies.

### 5.2. Bubble development at high dose

The results obtained here extend the model for the evolution of bubble structure with increasing helium dose (outlined in Section 2.1) into the high dose region where local helium concentrations exceed 20 at.%. For local helium concentrations approaching ≃20 at.% the bubble array still retains a cellular structure with most bubble cavities separated from their neighbours. At this stage there is a high degree of uniformity in the bubble array with typical bubble sizes about 3 to 4 nm. Continued implantation leads to a coarsening of the array and an increase in the degree of interconnection between bubbles. By the stage where the local helium concentrations are ≃30 at.%, the bubble size distribution has become bimodal. A population of large bubbles with typical dimensions in the range 30–80 nm coexists with a population of smaller bubbles with sizes in the range 3–5 nm. The smaller bubbles, which are in the columns separating the large bubbles, are not much larger than the uniform bubbles found at 20 at.%. This suggests that the coarsening of the bubble structure beyond 20 at.% takes place mainly in localised regions and it is bubble coalescence within these regions of enhanced bubble growth that lead to the formation of the large bubbles associated with radiation blistering.

### 5.3. Comparison of SEM and TEM results

The cavity structures revealed at the edges of blister lids and blister cavities under SEM match those in the heavily cavitated buried layer found in transverse sections using TEM. The SEM and TEM measurements of blister lid thickness agree and together indicate that the lid separates from the basement metal near the lower edge of the heavily cavitated layer. The debris left behind in crater floors, evident under SEM, is consistent with that expected from the TEM results and a cracking plane near the lower edge of the buried layer.

### 5.4. Deuteron induced blistering

As for helium, hydrogen isotopes such as deuterium are largely insoluble in copper. There have been several studies done of the blisters produced in copper and other metals by 200 keV deuteron irradiation at 120 K and subsequent heating to room temperature [20,21]. The classical blisters formed under deuterium implantation of copper at 120 K have a similar morphology to those found here for helium irradiation at 300 K. On heating deuterium-implanted targets to room temperature, widespread flaking of the surface occurred in most metals. SEM examination (at room temperature) showed blisters and flakes occurring together and in most metals several different depths of fracture were identified. TEM studies of underlying deuterium bubble structures were not attempted. In copper, two planes of fracture were observed. It was found that small classical blisters (≃ 7 μm across) formed first and that these had a consistently deeper plane of fracture than the blister flakes (≃30 μm across) that formed later. Once allowance is made for the difference in $R_p$ between the deuterium and helium cases, the depth of fracture for the deuterium blisters matches well that observed here for helium blisters. For the deeper of the two fracture planes in the deuteron blistering study, it was proposed that lateral shear stresses introduced by differential expansion, caused by a combination of radiation induced swelling and localised heating, played a central role in fracture. Explanations were also advanced for the origin of the fracture plane found at shallower depths. The existence of several different depths of fracture in a given metal would seem to indicate that, at a detailed level, there are several different mechanisms that can lead to blistering.

### 5.5. Re-examination of earlier studies

#### 5.5.1. Swelling

Surface displacement measurements [13,19,27] showed that the swelling was linear with dose, up to levels approaching the critical dose. For high doses, large values of swelling, ≃40% averaged over $2R_p$, were obtained. (This value agrees well with that found in Section 4.3.3, namely 40% averaged over $1.7R_p$.) The bubble structure observed under TEM in those studies accounted for only a small part of this swelling and it

was inferred that most of the swelling must have been associated with a sub-microscopic population of vacancies and vacancy clusters which were too small to image under TEM. The highly swollen bubble structures observed under TEM in the present work account for the high swellings observed in the early studies, entirely in terms of cavities with sizes greater than 2 nm. That the large cavities giving rise to most of the swelling have not been detected in previous studies, is attributed to differences in the methods used for preparing thinned sections for TEM examination. It can be inferred that, although present in the earlier studies, the heavily cavitated layer did not survive the thinning processes used to prepare TEM sections.

In terms of dose there are indications that the large bubbles observed here at high dose form relatively rapidly. Were this the case it would provide a ready explanation of the super-linear swelling that seemed to occur at doses close to the critical dose for radiation blistering in some surface displacement experiments – see, for example, [27,28].

It is interesting that the large swellings are accommodated by a global uplift of the surface rather than by local distortions of the surface to accommodate individual large bubbles. Although it is not known where the copper atoms displaced from cavities finally reside, it is clear that a major redistribution of metal atoms has occurred. Atom movements resulting from helium induced collisions may be important in this context. The calculated damage dose in the implanted layer (neglecting the build up of implanted helium) is estimated to be in the range 10–20 atomic displacements per atom (dpa) for helium dose levels approaching $\phi_c$. For such large local swellings it is probable that at least some of the atoms displaced from cavities must be accommodated locally in new atom planes, rather than undergo long range migration to distant sinks such as the surface or the substrate metal below the implanted layer. It seems that such new atom planes would have to preserve the local crystallography of the copper if the strain energy were not to exceed the local yield point of metal. Electron diffraction patterns (and bright field images) taken from the columns between the large bubbles indicate that the metal in the heavily implanted layer has largely retained its crystalline character.

*5.5.2. Suppression of blistering*

The early depth-profiling studies of Terreault and coworkers [1,5–7] showed that the profile of retained helium matched the calculated implantation profile up to the critical dose for radiation blistering. For copper near the critical dose, the helium concentration around the centre of the profile was found to drop suddenly (in terms of dose) from near 30 at.% down to just 6 at.%. The size of the decrease indicated that the helium lost from depths near $R_p$ must have come from almost the entire implanted layer, not just from the blister sites. (Assuming the fractional area covered by blisters was 30–40%, and that the helium was lost from the blister sites only, then the helium concentration would be expected to fall to 20 at.% and not to the 6 at.% that was observed.) An implication of these experiments would seem to be that helium has moved laterally to blister sites to escape through cracked lids at local helium concentrations near 30 at.%. In a related study, Scherzer et al. [29], made simultaneous measurements of blister formation and gas re-emission during bombardment of nickel with 8–40 keV helium ions at room temperature. It was shown that helium re-emission and blister formation start at the same critical fluence. One of their main conclusions was that the area contributing to gas re-emission was much larger than the blister area.

These results can be understood in terms of the bubble structures observed here. It could be expected that helium would move readily through a highly cavitated buried layer of the type evident in Fig. 5. In the regions between blisters, the direct movement of helium to the surface would be inhibited by the presence of the relatively undisturbed overlying layer and so the main movement would be laterally to blister sites. The size of the reduction in helium concentration at depths near $R_p$ found by Terreault et al. implies that at blistering all the helium is lost from the larger bubbles in this depth region. This suggests that these structures are permeable to helium and so could be described as nanoporous. In contrast it seems probable that in the columns between the large bubbles, the helium in the small bubbles making up the cellular structure continues to be retained. This proposal is supported by the observation by Terreault et al. that continued helium implantation beyond the critical dose for blistering tends to fill in the dip between the two peaks in the double-peaked distribution.

The early experiments showed that irradiation of metals to a critical dose of monoenergetic helium ions, at temperatures below about $0.5T_m$, resulted in blistering or flaking [13]. It was also known [6,13] that when the implantation profile was wide, e.g. in multiple energy implantations, or under variable angles of incidence, or at very low energy, surface deformation in the form of blistering and flaking was reduced or eliminated. The helium mobility was shown to be greatly enhanced when the helium concentration reached a threshold. The reduction in blistering was explained in terms of the helium-saturated layer extending to the surface to provide a pathway for release which prevented the build up of helium to the critical concentration required for blistering.

Evidence was found [6] suggesting that repetitive blistering could be circumvented if $R_p$ was less than 0.7 times the fwhm of the helium ion-end-of-range profile. This criterion was explained in terms of a permeable

layer (centred on the depth $R_p$) broadening to intersect the surface at a dose less than the critical dose for blistering. It was proposed that if this criterion were met, one generation only of blisters would be formed and that continued implantation would not result in further blistering. These features of blistering revealed in early experiments were explained originally [6] in terms of enhanced helium mobility through recrystallisation or percolation.

In 1982 Scherzer [13] reviewed all previous research on blistering. Particular consideration was given to the effects of particle reflection and surface regression owing to sputtering. It was concluded that two major conditions had to be met if blistering and flaking were to occur: (i) a critical concentration of gas, $C_{crit}$, had to be achieved in the metal, where $C_{crit}$ lies in the range 0.3–1.0 gas atoms per target atom and (ii) this critical concentration had to be reached first at a distance of at least several tens of nanometres from the surface. From this second criterion it was concluded that blistering and flaking would be suppressed if $C_{crit}$ was reached first at the surface and then continuously proceeded into the bulk.

The present results demonstrate that large values of swelling are associated with large bubbles forming in a buried layer below the surface, and that blistering finally occurs as the result of cracking of the metal columns between these large bubbles. It is interesting to interpret the above conditions for blistering in terms of the bubble structures found here. (The following discussion is limited to the case of helium implantation, since, as discussed in Section 5.4, there is evidence to suggest that for the implantation of other gases there may several different mechanisms that can result in blistering.) The early surface displacement measurements [27,28] showed that the degree of swelling increased monotonically with helium dose. (The dependence of swelling on dose was found to be linear at low and intermediate doses, with the possibility that there was an abrupt increase in the rate of swelling occurring as the critical dose for blistering was approached.) It follows that to produce a population of large bubbles of the type found here requires a particular helium concentration to be achieved in the implanted layer. In the present case, the threshold helium concentration for large bubble formation is estimated to lie in the range 0.3–0.5 helium atoms per metal atom. This concentration matches well the requirement on helium concentration for blistering proposed by Scherzer [13]. Similarly, the requirement that $C_{crit}$ must be reached first at depths of at least a few tens of nanometres, can be readily understood since if the bubble structure were produced at too shallow a depth the porous bubble layer could extend to the surface. It could be expected that this would result in helium escaping directly to the surface, rather than migrating laterally to incipient blister sites. In this way blistering would be pre-empted by gas loss to the surface.

*5.5.3. Physical properties*

The highly swollen buried layer shown in Fig. 5 could be expected to have quite unique mechanical, thermal and electrical properties. Whereas a detailed examination is beyond the scope of the present work some implications are outlined below.

Terreault and co-workers have provided convincing evidence that helium irradiation blisters in copper contain high-pressure gas. The leading model for gas-driven blistering is the inter-bubble fracture model proposed by Evans [30]. The model was developed on the basis that the final cracking that led to blistering took place between small ($\simeq$1 nm radius), regularly spaced, uniformly sized bubbles. This particular bubble structure was assumed for convenience and was not an essential component of the model. Wolfer [31], for example, has considered the model in relation to other bubble structures and equations-of-state for helium.

The bubble structure found here to be the immediate precursor to blistering involves two types of bubble populations. Fracture between the large bubbles would require cracking of the nanoporous columns between the large bubbles. This in turn requires cracking to occur in the metal between the small cavities (typical diameters about 4–8 nm) in the columns. For conventional pressure driven cracking, the crack tip radius would be expected to approximate to the radii of the small bubbles involved (i.e. $\simeq$3 nm). However, the copper 'walls' separating neighbouring small bubbles have a thickness equivalent to a few atom spacings only. It is not clear what the elastic and fracture properties of such thin lamellae would be. The plane of fracture in the present case is at a depth near the deeper boundary of the heavily cavitated buried layer. At this lower boundary the shear stresses between the highly swollen layer and the relatively undisturbed substrate could be expected to be at a maximum. This suggests that shear stresses may have an important role in the final cracking of the metal columns leading to blistering.

Yadava [18] has pointed out that the presence of subsurface bubbles can decrease the thermal conductivity of the implant/damage region by decreasing the mean free path of the heat carriers, electrons and phonons, owing to enhanced scattering. Throughout the implantation the beam power deposited in the implanted layer can be appreciable in experiments involving high current densities. In such cases, because of the increased impedance to heat flow from the implanted layer, the effective implantation temperature could be raised appreciably above the temperature of the substrate.

For the very highly swollen structures observed here, the effective thermal conductivity could be expected to differ appreciably from macroscopic values. Not only are the mean free paths for electron (and phonon) scattering appreciably reduced but also there is a large reduction in the cross-sectional area of metal available

for heat conduction. The beam power in the present study was relatively low (typically several W $cm^{-2}$) and so it is thought that any temperature rises in the implanted layer would not have been large except, perhaps, in the very last stages of blistering. This is supported by the observation that the smaller bubbles (in the metal columns separating the large bubbles) in micrographs such as Fig. 5, show no obvious signs of thermally driven growth. Given this, it is interesting that the large bubbles do bear some similarity (in terms of size, concentration and facetting) to the bubbles produced by the post-irradiation thermal annealing of targets implanted to a lower dose level [25,26].

### 5.6. CTR first wall

The degree of blistering and flaking, and blister morphology, depend sensitively on a number of factors associated with the incident helium flux as well as on the temperature of the metal. These factors include the mean energy, the flux density, and the spread in energies and angles of incidence of the primary flux. The implantation conditions used here are not those expected at the first-wall of future plasma devices under normal operating conditions. However, there is the potential for the processes identified here to occur in some localised regions, for example, in the cooler parts of exposed surfaces, or in areas exposed to atypical flux conditions.

Perhaps more importantly, the results obtained provide new insights into underlying mechanisms and possibilities for exotic microstructural development under the extreme conditions prevailing in energetic inert gas implantations. In this sense the results relate directly to assessing the likelihood of the development of porosity. Furthermore, they contribute to the knowledge base needed to assess the potential for preconditioning metal walls, by prior implantation, to produce blister resistant equilibrium surfaces with desirable gas-loading and thermal properties.

## 6. Conclusion

Transverse TEM sections (i.e. sections perpendicular to the implanted surface) can be successfully prepared by means of ultramicrotomy from copper implanted with helium even to a dose level beyond the critical dose for radiation blistering of the target surface. For a dose level equal to the critical dose, the metal in the implanted layer is highly swollen, with local swellings estimated to exceed 150% owing to the presence of a bimodal distribution of nanoscale bubbles. That these highly swollen structures have not been seen in earlier TEM studies is attributed to the chemical techniques used for specimen thinning. It could be expected that chemical erosion would preferentially attack the highly swollen structures to the extent that these structures would not survive the thinning process. In respect of using inert gas implantation for tailoring uniform nanoporous surfaces for use in applications it is concluded that blistering may set the upper useful dose limit for high-energy monoenergetic implantations.

The structure and depth dependence of the bubble arrays directly associated with radiation blistering have been determined for the particular case of helium ion implantation in copper at temperatures around $\simeq 0.2T_m$. Much of the swelling is contributed by large bubbles (30–80 nm across) formed in high concentration in a buried layer. The metal in the columns separating these large bubbles contains a high concentration of smaller bubbles (3–5 nm across). A characteristic of both bubble populations is the small spread in bubble sizes. These observations provide a ready explanation for some previously puzzling aspects of the earlier studies of radiation blistering. Examples of earlier results that can now be explained include: (i) the high values of swelling revealed by surface displacement measurements, (ii) the existence of a threshold dose for enhanced helium mobility, (iii) the double-peaking of helium depth-profiles near blistering, and (iv) the suppression of blistering in cases where the heavily implanted layer extends to the surface.

## Acknowledgements

This work was performed under a research contract to the New Zealand Foundation for Research, Science and Technology. We thank Dr P.W. Gilberd for useful discussions, Yvonne Morrison for research assistance and Tong Young and Piers Chamberlain for providing accelerator support. We thank Dr D.J. Mazey and Dr J.H. Evans formerly of AEA Reactor Services, Harwell Laboratory, UK, for stimulating discussions on bubble structures.

## References

[1] P.B. Johnson, in: J.H. Evans, S.E. Donnelly (Eds.), Fundamental Aspects of Inert Gases in Solids, Plenum, New York, 1991, p. 167.
[2] P.W. Gilberd, P.B. Johnson, I.C. Vickridge, Nucl. Instrum. and Meth. B 127&128 (1997) 738.
[3] P.W. Gilberd, P.B. Johnson, I.C. Vickridge, A.C. Wismayer, J. Nucl. Mater. 244 (1997) 51.
[4] P.B. Johnson, P.W. Gilberd, Nucl. Instrum. and Meth. B 127&128 (1997) 734.
[5] B. Terreault, R.G. Saint-Jacques, G. Veilleux, J.G. Martel, J.L. Ecuyer, C. Brassard, C. Cardinal, Canadian J. Phy. 56 (2) (1978) 235.
[6] B. Terreault, J. Nucl. Mater. 93&94 (1980) 707.

[7] B. Terreault, G. Ross, R.G. Saint-Jacques, G. Veilleux, J. Appl. Phys. 51 (3) (1980) 1491.
[8] P.B. Johnson, D.J. Mazey, J. Nucl. Mater. 218 (1995) 273.
[9] P.B. Johnson, D.J. Mazey, J. Nucl. Mater. 170 (1990) 290.
[10] K.J. Stevens, P.B. Johnson, J. Nucl. Mater. 246 (1997) 17.
[11] F.E. Lawson, P.B. Johnson, J. Nucl. Mater. 252 (1998) 34.
[12] P.B. Johnson, Karen L. Reader, R.W. Thomson, J. Nucl. Mater. 231 (1996) 92.
[13] B.M.U. Scherzer, Sputtering by particle bombardment part II, in: R. Behrisch (Ed.), Topics in Applied Physics, Springer, Berlin, vol. 52, 1982, pp. 271–355.
[14] A.A. Lucas, Physica 127B (1984) 225.
[15] K. Krishan, Radiat. Eff. 66 (1982) 121.
[16] J.H. Evans, in: R.W. Cahn (Ed.), Encyclopaedia of Materials Science and Engineering, Suppl. vol. 1, Pergamon, Oxford, 1988, p. 547.
[17] J.H. Evans, in: D. Walgraef, N.M. Ghoniem (Eds.), Proceedings of the NATO Advanced Study Institute on Patterns, Defects and Instabilities, Cargese, Corsica, Sept., 1989, Kluwer Academic, Dordrecht, 1990, p. 347.
[18] R.D.S. Yadava, Radiat. Eff. 63 (1982) 231.
[19] G. Veilleux, R.G. Saint-Jacques, J. Nucl. Mater. 103&104 (1981) 421.
[20] P.B. Johnson, T.R. Armstrong, Nucl. Instrum. and Meth. 148 (1978) 85.
[21] P.B. Johnson, W.R. Jones, J. Nucl. Mater. 120 (1984) 125.
[22] W.R. Jones, P.B. Johnson, J. Nucl. Mater. 144 (1987) 157.
[23] P.B. Johnson, D.J. Mazey, J. Nucl. Mater. 111&112 (1982) 681.
[24] J.F. Ziegler, J.P. Biersack, U. Littmark, The Stopping and Range of Ions in Matter, Pergamon, New York, 1985.
[25] P.B. Johnson, D.J. Mazey, Radiat. Eff. 53 (1980) 195.
[26] P.B. Johnson, D.J. Mazey, J.H. Evans, Harwell report AERE R-10874 (1983), Radiat. Eff. 78 (1983) 147.
[27] R.S. Blewer, W. Beezhold, Radiat. Eff. 19 (1973) 49.
[28] R.G. Saint-Jacques, G. Veilleux, B. Terreault, Nucl. Instrum. and Meth. 170 (1980) 461.
[29] B.M.U. Scherzer, J. Ehrenberg, R. Behrisch, Radiat. Eff. 78 (1983) 417.
[30] J.H. Evans, J. Nucl. Mater. 61 (1976) 1.
[31] W.G. Wolfer, J. Nucl. Mater. 93&94 (1980) 713.